PAN
ARCHIVES OF ACOUSTICS
Vol. **45**, No. 3, pp. 459–465 (2020)
DOI: 10.24425/aoa.2020.134062

Research Paper

Two-Phase Flow Measuring with Ultrasonic Tomography

Omid QORBANI, Esmaeil Najafi AGHDAM*

Sahand University of Technology
Faculty of Electrical Engineering
Tabriz, Iran; e-mail: e_qorbani@sut.ac.ir
*Corresponding Author e-mail: najafiaghdam@sut.ac.ir

(*received December 2, 2019; accepted April 7, 2020*)

The exact measurement of multiphase flow is an important and essential task in the oil and petrochemical related industries. Several methods have already been proposed in this field. In the existing methods, flow rate measurement depends on the fluid flow pattern. Flow pattern recognition requiring calibration has created instability in such systems. In this paper, a imple and reliable method is proposed which is based on ultrasonic tomography. It is free from calibration and instability problems that existing methods have. The obtained data from a 32-digit array of ultrasonic sensors have been used and the two-phase flow rate including liquid and gas phases have been calculated through a simple algebraic algorithm. Simulation results show that while applying this method the measurement technique is independent from the fluid flow pattern and the system error is decreased. For the proposed algorithm, the average amount of the spatial imaging error (SIE) for a bubble at different positions inside the pipe is about 5%.

Keywords: two-phase flowmeter; ultrasonic flowmeter; ultrasonic tomography.

1. Introduction

Nowadays the multiphase flow measurement is a big challenge in gas and petroleum industries. In such industries, multiphase flowmeters are used for reservoir management, controlling the process of injecting chemical materials into the reservoir, acidification, and optimising the production from oil reservoir (Ismail, 2005; Kirillov, 2014; Safonov, 2014; Wahab, 2011; Zhang, 2014). Multiphase flowmeters show fluid online variations. In the past, oil separation was used for calculating flow rate of reservoir output, but due to the large size of equipment, high cost of maintenance, and their long delay in showing fluid flow variations, the tendency to use multiphase flowmeters instead of separators has grown (Thorn *et al.*, 2012).

Multiphase or two-phase flowmeters can be divided into two categories: invasive and noninvasive ones (Xu, Xu, 1997; Wang *et al.*, 2015). Pitot tube, Orifice, V-cone, or turbines belong to invasive measurement where the tools are placed inside the pipe and remain in contact with the fluid. The main problem with these tools is friction with the fluid which causes the variation of fluid flow pattern and decreases the accuracy of the system; also the lifetime of such tools is shorter than that of noninvasive tools. X-ray, gamma-ray, radioactive sensors, ultrasonic and magnetic waves can be categorised as noninvasive measurement tools. Noninvasive flow rate measurement is better than other methods but it has some disadvantages. Noninvasive optical method and using transparent pipes have a high speed response but the transparency of the pipe and media are their severe limitations. Nonlinear electrical properties of the soft media are disadvantages of measurement systems based on electrical properties (Xu, Xu, 1997; Liang *et al.*, 2016). On the other hand, the method based on X-rays, gamma rays, and radioactive sensors have high fabrication and maintenance cost. Also these methods may be harmful to workers.

Ultrasonic waves are applied in a wide range of areas such as medical imaging, fluid flow measurement, and flaws detecting, but they also have some limitations such as slow propagation velocity and temperature dependence (Wang *et al.*, 2015; Camacho *et al.*, 2012; Opieliński, 2013). In flow measurement based on ultrasonic waves, central frequency must be selected appropriately to achieve requested precision. Moreover, compared with optic and electromagnetic waves, ultrasonic waves consume less energy, their mainte-

nance cost is lower, and their scale-up is performed easily (Rahiman *et al.*, 2010). Flow measurement by ultrasonic waves was studied and developed for the first time in 1980 and was implemented in the field in 1990 (Xu, 1997). The common method of two-phase flow measurement with ultrasonic waves use transient time technique and/or Doppler effect. Recently, artificial intelligence and mathematical algorithms are used for analysing sensor's outputs and measuring flow rate (Koike, 2002; Rahim, 2007; Wang, 2003). In general, gas and liquid flow pattern varies with pressure, temperature, the geometric figure of pipes, or amount of flow rate (Kumar, 2015). One of the most important disadvantages of those techniques is that measurement depends on fluid flow patterns and then causes instability in the system. Also, recognition of these patterns by multiple sensors requires complicated algorithms. Thus, these systems should be equipped with permanent calibration that might be used for one special kind of flow pattern (Bratland, Ove, 2010).

Tomography can be used to solve the abovementioned problems about two-phase flowmeters and to simplify fluid flow measurement. Tomography has a wide range of applications in biotechnology and medical industries and the operation of reactors (Wahab, 2011; Rokhana, Anggraini, 2015). There are various methods and sensors for tomography such as X and gamma rays, Ionizing Radiation, Position-Emission Tomography (PET), Nuclear Magnetic Resonance (NMR), sound and electrical methods (using impedance and capacitor properties of media) (Liang *et al.*, 2016; Wang, 2015).

Tomography is a process for creating two-dimensional images from a three-dimensional object and it can provide a cross-sectional image of fluid distribution inside the pipe. Nondestructive, noninvasive, less expensive, and online operation are the key benefits of ultrasound tomography (Wang, 2015). Ultrasound tomography is comprised by ultrasonic transient time tomography (UTT) and ultrasonic reflection mode tomography (URT). We can use both the UTT and URT for multiphase flow processing. Combining UTT and URT results for reconstruction algorithm gives us many advantages, which is better than the single modality of UTT or URT (Tan *et al.*, 2019).

In the previous papers, ultrasonic tomography has been used for recognising fluid flow pattern, fluid behaviour inside the pipe, etc. (Ismail, 2005; Wahab, 2011; Xu, Xu, 1997; Wang, 2003; Besic, 2014). One of the most important ultrasonic tomography applications is in the medical imaging. Ultrasound tomography enables early detection of pathologies in biological tissues. An ultrasonic array can be used for tomography too. We can change the inclination and focusing of the waves by changing the activation time of the ultrasonic transducers (Staszewski *et al.*, 2019). Thus, considering its potential, the ultrasonic tomography will be used in this paper for two-phase flow rate measurement.

2. Principle and construction

Transmission and reflection modes are used for ultrasonic tomography with physical properties related to the time of flight and Doppler effect, respectively. We can use one of these modes for ultrasonic tomography but in some cases both the transmission and reflection modes are used for enhancing UT precision (Tan *et al.*, 2019). The sensor's output data is using for reconstructing cross-sectional image of fluid inside the pipe, fluid flow obtained from image processing, and fluid motion velocity. There are various algorithms for image reconstruction depending on sensors data, therefore algorithm selection depends on the kind of sensors in the tomography (Dobrucki, Opieliński, 2000). Zernike multinomial (Besic, 2014), ellipse algorithm (Yang, 2013), and back projection algorithm (Tan *et al.*, 2019; Nordin, 2014) are examples of such algorithms.

The presented method is based on acoustic impedance difference between gas and liquid which causes wave return on the interface between two phases (Wahab, 2011; Rahiman *et al.*, 2008):

$$R_p = \frac{Z_2 - Z_1}{Z_2 + Z_1}, \tag{1}$$

$$T_p = \frac{2Z_2}{Z_2 + Z_1}. \tag{2}$$

In the above relation, R_p, T_p, Z_1 and Z_2 indicate ultrasound pressure reflection, transmission coefficients, and acoustic impedance of the media, respectively. According to these relations, the amount of pressure reflection from the interface of gas (air) and liquid (water) is 99.94%. Table 1 shows impedance values and sound speeds for air and water (Liang *et al.*, 2016). Wave reflection value in the interface of two phases can be calculated by considering the acoustic impedance of phases.

Table 1. Density, sound speed, and acoustic impedance at normal temperature (27°C) and pressure.

Media	ρ [kg/m^3]	c [m/s]	Z [Mrayl]
Water	1000	1497	1.497
Air	1.293	346	0.00045

To select the piezoelectric centre frequency for water media, we use the relation $\frac{2\pi}{\lambda}\alpha \gg 1$ (Xu, Xu, 1997), where α and λ are the bubble radius inside the pipe and sound wavelength, respectively. For instance, for a piezoelectric sensor with 2 MHz centre frequency, a bubble with a 1.2 mm diameter can be recognised.

For fluid speed measuring by an ultrasonic wave in the pipe, we can use a Fig. 1 configuration where ul-

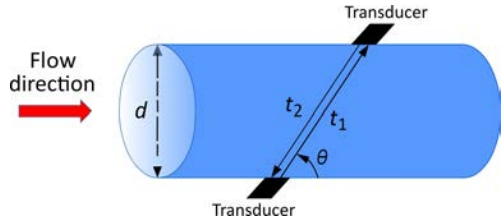

Fig. 1. Schematic of sensors arrangement on the pipe for flow velocity measurement.

trasonic signals are emitted and received by two transducers. The flow velocity can be achieved with propagation delay time between flow direction and opposite direction.

In the normal pressure and temperature, we can suppose that both phases of flow have the same speed and we can neglect the slip effect for the gas phase. In this condition velocity of the fluid flow is given by the following equation (Xing, 2014):

$$V = \frac{d}{\sin(2\theta)}\left(\frac{1}{t_1} - \frac{1}{t_2}\right), \tag{3}$$

where t_1, t_2, and d are propagation time in path 1 and path 2, and diameter of the pipe, respectively, and θ is the ultrasonic incident angle into the pipe. In the room conditions, while the fluid flow is not turbulent, the bubbles inside the liquid can be assumed as convex. Besides, if the transmitted ultrasound wavelength are small compared with the bubble diameter, the motion of the waves is considered in a direct line. Therefore, we can use the fan-shaped scan technique for piezoelectric sensors arrangement.

In the fan-shaped arrangement, all of the sensors can transmit and receive an ultrasonic wave and this process is controlled by the electronic circuits (Fig. 2). By considering ultrasonic wave movement in the direct line, if there is a gas bubble between two piezoelectric sensors in the direct path, the receiver will not receive any signal in the specified time because in this condition the wave scatters from bubble surface, and if the path includes only water phase, the signal is received at specified time with acceptable amplitude. The piezoelectric receiver may receive various ultrasonic signals (from different paths) at the same moment and this can cause incorrect recognition of the target signal. To solve this we have limited the signal reception time by target sensor (based on the exact position of piezoelectric sensors on the pipe and velocity of wave in the liquid phase). It means that the tomography technique is based on signal reception time and signal level, thus the waves which arrived after reflection from other paths have not been received (Fig. 3).

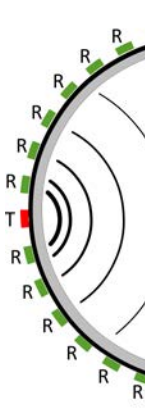

Fig. 2. Fan-shaped sensors arrangement.

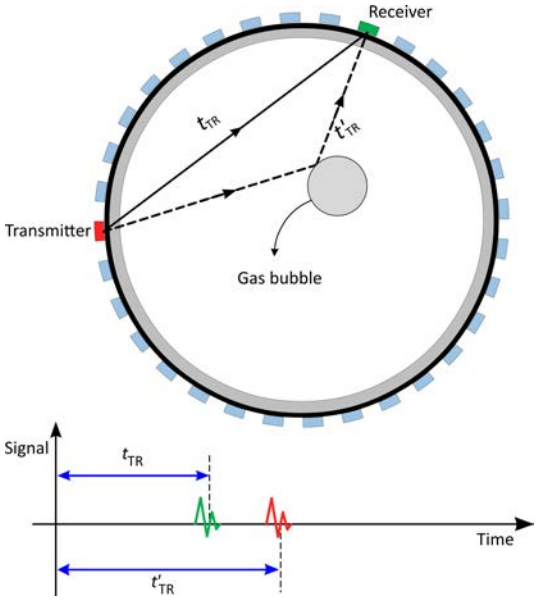

Fig. 3. Cross-sectional image of the bubble.

After completion of transmission and reception by all of the piezoelectric sensors, the first shot is formed and after a short delay that has been set for sensitivity matrix formulation and ultrasound waves settling, the next shot will be captured. Figure 4 shows the shot with a cross-sectional image of the gas bubble inside the pipe.

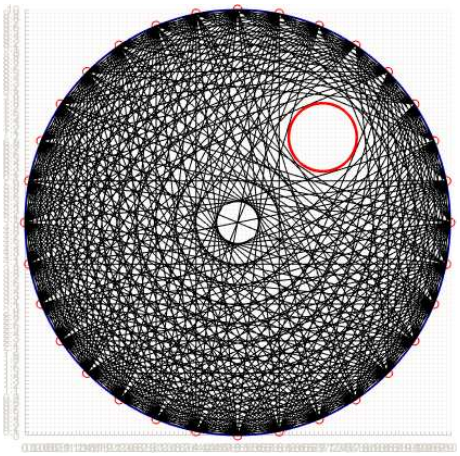

Fig. 4. Propagation time difference between two paths.

Output of driver circuit includes signals with two major and minor frequencies. Major frequency is adjusted with respect to the time needed for transmission and reception between piezoelectric sensors; thus it is equal to the number of shots of fluid flow in one second. Minor frequency is the central frequency of piezoelectric (Fig. 5) (Kirillov, 2014). We can calculate major frequency with the equation that follows and from the t for an ultrasonic reflection system:

$$t = n\frac{2d}{v}(1+p), \tag{4}$$

where n is the number of transducers, d is the pipe diameter, v is the sound speed in the media, and p is an additional percentage of time for the ultrasonic wave to attenuate below a detectable level (Wang, 2015).

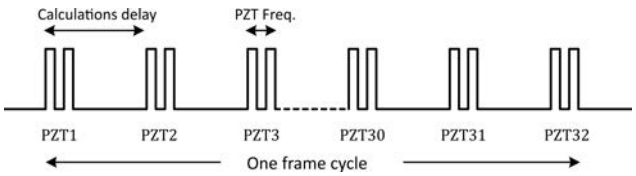

Fig. 5. One frame of the tomography cycle.

Here, receiver output is considered as two signal levels of zero and one, so that if the signal is received, the output becomes one, and if there is no signal, it is considered zero. Therefore, if the number of piezoelectric sensors is n, the data obtained from them in one shot are calculated as $n \times n$ matrix. This matrix is called the sensitivity matrix and its main diameter is defined as null (because piezoelectric sensor cannot be transmitter and receiver simultaneously). In addition, the sensitivity matrix is symmetrical relative to the main diameter. The sensitivity matrix is used for the reconstruction of cross-sectional image of the pipe. The most common algorithm for reconstructing an image from the sensitivity matrix is the back projection algorithm (Wang, 2015). Sensitivity matrix processing algorithms and image processing both have systematic error and therefore, in the worst case, these errors are added to the error of sensors. In our method, the sensitivity matrix has been used for acquiring gas and liquid flow amount directly, without image processing. The important point in flow computation is that multiphase fluid pattern inside the pipe changes slowly (Liang *et al.*, 2016), therefore flow patterns can be considered constant in a relatively long period. Thus, in this method, there is no need to recognise fluid flow patterns or perform system calibration.

3. Proposed method

The presented method for measuring two-phase fluid flow is divided into two sections. First, with respect to initial data, the pipe diameter, the number, and place of piezoelectric sensors, the cross-section of the pipe is divided into small pixels just like it is done in the Computational Fluid Dynamics (CFD) based software. The number of pixels is different depending on the pipe diameter and piezoelectric number. In the back projection algorithm for image reconstruction with a growing number of sensors we cannot achieve high resolution and enlarging the size of the image grid does not help (Opielinski, Gudra, 2006). However, in the proposed method we can improve precision of the measurement by increasing the number of sensors and pixels of the gridded area. We mesh the pipe vertical slice and according to the exact place of the mounted piezoelectric sensors, pixels located in the path between two sensors are calculated.

For example, Fig. 6 shows pixels located in the direct path between two sensors. In order to count the pixels correctly, every pixel is numbered inside the pipe. After computing these data for all pairs of the sensors, the data are stored in the $n \times n$ table so that in the (i, j)-th home of the table there is a $1 \times k$ matrix which includes all of the pixels located in the path between sensor i and j. These data are constant for an installed system and they only depend on the arrangement of sensors and meshing manner of pipe cross-section.

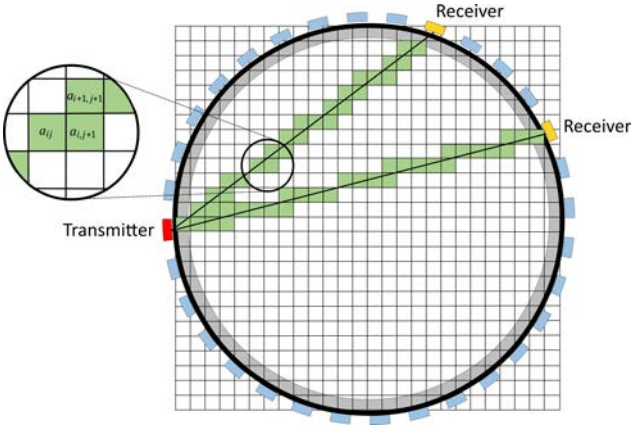

Fig. 6. Pixel finding algorithm.

Moreover, the above mentioned table is calculated only once, before the flowmeter start up. The primary table is a symmetrical table.

The second section is concerned with the computation of cross-section area of each phase inside the pipe by using the data of sensors. As we mentioned in the previous section, in each shot or sonogram, the related sensor's data are stored in a sensitivity matrix. Here, if an ultrasonic wave is received in the piezoelectric sensor (voltage observation), this piece of data is considered as 1, and otherwise, it is stored as 0. This kind of digitalisation of data results in simple computation and error reduction. After acquiring the sonogram data, the computation of inside-pipe flow begins. In this computation, if (i, j)-th sensitivity matrix entry

was 1, the pixels that were stored in the primary table will be supposed as water pixels. In addition, if other arrays in the sensitivity matrix were 1, new pixels will be added to the water pixels set. The most important point here is that the addition should be done as a set union operator. The numbering of the pixels has been done for pixel uniqueness and applicability of union syntax in the MATLAB. After finishing the processing of sensitivity matrix arrays, the water pixels are specified. All of these pixels are 100% water because if there was gas in the path of the sensors, the related pixels would count zero. Therefore, the percentage of water inside the pipe is obtained through counting the number of pixels in this set and dividing it into the total number of pixels in the pipe cross-section. In the presented method for computing gas percentage and with respect to Fig. 7, a real cross-section of the gas bubble is always smaller than the calculated value. Then, according to the sensitivity matrix, we obtain the biggest polygon inside the cross-section and consider the average surface of two polygons for the size of the gas bubble.

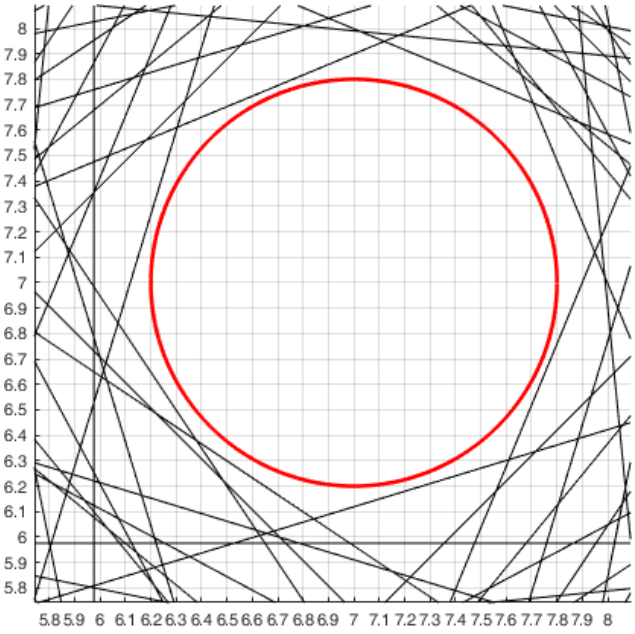

Fig. 7. Circumscribed polygon of the gas bubble.

By supposing that gas bubble cross-section in tomography image is A and pipe cross-section is B, the volume of gas flowing through the pipe in the image reconstruction time is $A \cdot V \cdot \Delta t$ and for the liquid phase it equals $(B-A) \cdot V \cdot \Delta t$, where V is the fluid movement velocity inside the pipe and Δt is the image reconstruction time shown in Fig. 4 as calculation delay time. The momentary flow of gas and liquid are calculated as follows and flow of each phase is obtained by summing them in the time domain

$$q_l = (B - A) \cdot V \cdot \Delta t, \tag{5}$$

$$q_g = A \cdot V \cdot \Delta t, \tag{6}$$

$$Q_g = q_{g1} + q_{g2} + \ldots + q_{gn} = \sum_{i=1}^{n} q_{gi}, \tag{7}$$

$$Q_l = q_{l1} + q_{l2} + \ldots + q_{ln} = \sum_{i=1}^{n} q_{li}, \tag{8}$$

where n is the number of sonograms in the tomography and Q_g, Q_l are the volumes of the gas and liquid flows, respectively.

4. Simulation results

Spatial imaging error (SIE) parameter is used for studying the precision of simulations. This parameter is considered as including total error of the set and calculated as follows (Xu, Xu, 1997):

$$\mathrm{SIE} = \frac{\sum_{i=1}^{L} \sum_{j=1}^{L} |G_s(i,j) - G_r(i,j)|}{\sum_{i=1}^{L} \sum_{j=1}^{L} G_s(i,j)}, \tag{9}$$

where

$$G_s(i,j) = \begin{cases} 1 & \text{at pixels processed} \\ & \text{by bubble models,} \\ 0 & \text{elsewhere,} \end{cases} \tag{10}$$

and

$$G_r(i,j) = \begin{cases} 1 & \text{at pixels processed} \\ & \text{by reconstruction bubble,} \\ 0 & \text{elsewhere,} \end{cases} \tag{11}$$

or in the proposed method

$$\mathrm{SIE} = \frac{\text{reconstructed bubble surface}}{\text{real surface of bubble}}. \tag{12}$$

It is evident that the closer this number to 1, the higher the precision shown by the system. To study the precision of the algorithm, we consider a gas bubble in various situations inside the pipe and compute the SIE factor. We have chosen the radius of the pipe and bubble as 5 and 0.6 in unit scale, respectively, and bubble situations were chosen in the first quarter of a coordinate circle with steps one-tenth in X and Y directions. A 32-number array on the outer wall of the pipe has been used for sensors arrangement. The results of the simulation are depicted in Figs 8 and 9 with the vertical axis being the spatial imaging error (SIE) factor value and the horizontal axis corresponding to the bubble centre position inside the pipe, and the maximum error in image reconstruction algorithm occurs in the centre of the pipe. This error varies with bubble size and location but we can reduce it with increasing the number of sensors and verifying the algorithm.

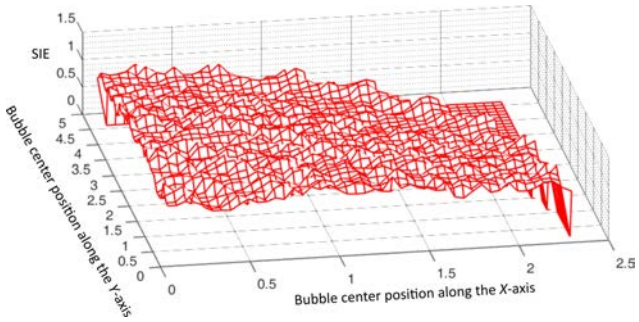

Fig. 8. SIE error calculating by gas bubble displacement.

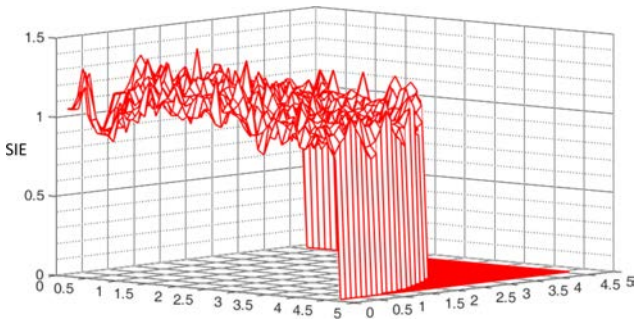

Fig. 9. SIE error in the first quarter.

5. Conclusion

The key benefits of ultrasound tomography (UT) are that it is non-destructive, non-invasive, uses no moving parts, and can be an online operation. UT is often less expensive than other techniques. Ultrasound transient time and ultrasound pressure reflection are used for ultrasound tomography. The proposed method can be applied for two-phase flow measurement with Ultrasonic Tomography. We have utilised a new algebraic method for two-phase fluid flow measurement. The flow measurement system has no need for artificial intelligence, complicated mathematical algorithms, and calibration systems. In addition, this method does not need to recognise the flow pattern, so the system will be very stable. Based on the simulation results, the accuracy of the proposed method is acceptable. The proposed method is very simple and it doesn't require sophisticated hardware or software, which will contribute to the speed of the measuring system. For the proposed algorithm, the average amount of the SIE factor for a bubble at different positions inside the tube is about 5%. The size of pixels in the proposed method depends on the number of sensors and we can enhance the method's precision by enlarging it. The number of pixels is not dependent on the size of the tube and it only depends on the number of sensors. In the measuring algorithm, if the centre of the bubble lies on the axis of the tube, measurement error can probably increase. The error varies with the bubble radius. For the future work, we need to set up the lab-scale configuration to verify the algorithm's precision.

References

1. Besic N. *et al.* (2014), Zernike ultrasonic tomography for fluid velocity imaging based on pipeline intrusive time-of-flight measurements, *IEEE Transactions on Ultrasonics, Ferroelectrics, and Frequency Control*, **61**(11): 1846–1855, doi: 10.1109/TUFFC.2014.006515.
2. Bratland O. (2010), *Pipe flow 2: multi-phase flow assurance*, pp. 41–59, http://drbratland.com/PipeFlow2/.
3. Camacho J., Medina L., Cruza J.F., Moreno J.M., Fritsch C. (2012), Multimodal ultrasonic imaging for breast cancer detection, *Archives of Acoustics*, **37**(3): 253–260, doi: 10.2478/v10168-012-0033-4.
4. Dobrucki A.B., Opieliński K.J. (2000), Adaptation of image reconstruction algorithm for purposes of ultrasound transmission tomography (UTT), *Archives of Acoustics*, **25**(4): 395–422, https://acoustics.ippt.pan.pl/index.php/aa/article/view/378/316.
5. Ismail I., Gamio J.C., Bukhari A.S.F., Yang W.Q. (2005), Tomography for multi-phase flow measurement in the oil industry, *Flow measurement and instrumentation*, **16**(2–3): 145–155, doi: 10.1016/j.flowmeasinst.2005.02.017.
6. Kirillov K.M., Nazarov A.D., Mamonov V.N., Serov A.F. (2014), An ultrasonic flowmeter for viscous liquids, *Measurement Techniques*, **57**(5): 533–536, doi: 10.1007/s11018-014-0492-2.
7. Koike Y., Tsuyoshi T., Kikura H., Aritomi M., Mori M. (2002), Flow rate measurement using ultrasonic Doppler method with cavitation bubbles, [in:] *2002 IEEE Ultrasonics Symposium, Proceedings*, Vol. 1, pp. 531–534, doi: 10.1109/ULTSYM.2002.1193458.
8. Kumar K., Swain T.K., Ekhande C.S., Nanawaare R.M. (2015), Effects of flow measurement on sloped pipes using ultrasonic flowmeter, [in:] *2015 International Conference on Industrial Instrumentation and Control (ICIC)*, pp. 1490–1494, doi: 10.1109/IIC.2015.7150985.
9. Liang F., Zheng H., Yu H., Sun Y. (2016), Gas–liquid two-phase flow pattern identification by ultrasonic echoes reflected from the inner wall of a pipe, *Measurement Science and Technology*, **27**(3): 035304, doi: 10.1088/0957-0233/27/3/035304.
10. Nordin N., Idroas M., Zakaria Z., Ibrahim M.N. (2014), Tomographic image reconstruction of monitoring flaws on gas pipeline based on reverse ultrasonic tomography, [in:] *2014 5th International Conference on Intelligent and Advanced Systems (ICIAS)*, pp. 1–6, doi: 10.1109/ICIAS.2014.6869445.
11. Opielinski K.J., Gudra T. (2006), Recognition of external object features in gas media using ultrasound transmission tomography, *Ultrasonics*, **44**: e1069–e1076. doi: 10.1016/j.ultras.2006.05.102.

12. Opieliński K.J. *et al.* (2013), Ultrasound transmission tomography imaging of structure of breast elastography phantom compared to US, CT and MRI, *Archives of Acoustics*, **38**(3): 321–334, doi: 10.2478/aoa-2013-0039.

13. Rahiman M.F., Rahim R.A., Zakaria Z. (2008), Design and modelling of ultrasonic tomography for two-component high-acoustic impedance mixture, *Sensors and Actuators A: Physical*, **147**(2): 409–414, doi: 10.1016/j.sna.2008.05.024.

14. Rahiman M.H.F., Rahim R.A., Ayob N.M.N. (2010), The front-end hardware design issue in ultrasonic tomography, *IEEE Sensors Journal*, **10**(7): 1276-1281, doi: 10.1109/JSEN.2009.2037602.

15. Rahim R.A., Rahiman M.F., Chan K.S., Nawawi S.W. (2007), Non-invasive imaging of liquid/gas flow using ultrasonic transmission-mode tomography, *Sensors and Actuators A: Physical*, **135**(2): 337–345, doi: 10.1016/j.sna.2006.07.031.

16. Rokhana R., Anggraini S. (2015), Using of array of 8 ultrasonic transducers on acoustic tomography for image reconstruction, [in:] *2015 International Electronics Symposium (IES)*, pp. 20–25, doi: 10.1109/IIC.2015.7150985.

17. Safonov A. (2014), Experience with the use of ultrasonic flowmeters in systems for measuring the quantity and quality of petroleum, *Measurement Techniques*, **57**(4): 458–460, doi: 10.1007/s11018-014-0477-1.

18. Staszewski W., Gudra T., Opieliński K.J. (2019), The effect of dynamic beam deflection and focus shift on the acoustic field distribution inside the ultrasonic ring array, *Archives of Acoustics*, **44**(4): 625–636, doi: 10.24425/aoa.2019.129721.

19. Tan C., Li X., Liu H., Dong F. (2019), An ultrasonic transmission/reflection tomography system for industrial multiphase flow imaging, *IEEE Transactions on Industrial Electronics*, **66**(12): 9539–9548, doi: 10.1109/TIE.2019.2891455.

20. Thorn R., Johansen G.A., Hjertaker B.T. (2012), Three-phase flow measurement in the petroleum industry, *Measurement Science and Technology*, **24**(1): 012003, doi: 10.1088/0957-0233/24/1/012003.

21. Wahab Y.A., Ahmad M.A., Rahim R.A., Rahiman M.F. (2011), Application of transmission-mode ultrasonic tomography to identify multiphase flow regime, [in:] *International Conference on Electrical, Control and Computer Engineering (InECCE)*, pp. 119–123, doi: 10.1109/INECCE.2011.5953861.

22. Wang M. [Ed.] (2015), *Industrial tomography: systems and applications*, Woodhead Publishing, doi: 10.1016/C2013-0-16466-5.

23. Wang T., Wang J., Ren F., Jin Y. (2003), Application of Doppler ultrasound velocimetry in multiphase flow, *Chemical Engineering Journal*, **92**(1–3): 111–122, doi: 10.1016/S1385-8947(02)00128-6.

24. Xing L. *et al.* (2014), A combination method for metering gas–liquid two-phase flows of low liquid loading applying ultrasonic and Coriolis flowmeters, *Flow Measurement and Instrumentation*, **37**: 135–143, doi: 10.1016/j.flowmeasinst.2014.01.005.

25. Xu L., Han Y., Xu L.A., Yang J. (1997), Application of ultrasonic tomography to monitoring gas/liquid flow, *Chemical Engineering Science*, **52**(13): 2171–2183, doi: 10.1016/S0009-2509(97)00043-2.

26. Xu L.J., Xu L.A. (1997), Gas/liquid two-phase flow regime identification by ultrasonic tomography, *Flow Measurement and Instrumentation*, **8**(3–4): 145–155, doi: 10.1016/S0955-5986(98)00002-8.

27. Yang L., Pan Q., Xu C., Guo X., Peng K. (2013), Immersion ultrasonic reflection tomography by annular array system, [in:] *2013 Far East Forum on Nondestructive Evaluation/Testing: New Technology and Application*, pp. 82–89, doi: 10.1109/FENDT.2013.6635534.

28. Zhang R., Wang Q., Wang H., Zhang M., Li H. (2014), Data fusion in dual-mode tomography for imaging oil–gas two-phase flow, *Flow Measurement and Instrumentation*, **37**: 1–11, doi: 10.1016/j.flowmeasinst.2014.03.003